PHYSICS 598 CPA : Problem Set 10

Ricky Chue

1 Linear Elliptic PDE

Solve

$$\frac{\partial^2 u}{\partial x^2} + \frac{\partial^2 u}{\partial y^2} = \rho$$

inside a 32×32 square lattice, with spacing $\Delta = 1/32$ and $\rho = 2$ in the center ($j = l = 16$) and zero everywhere else. The finite difference equation is:

$$u_{j+1,l} + u_{j-1,l} + u_{j,l+1} + u_{j,l-1} - 4u_{j,l} = \rho_{j,l}\Delta^2$$

Solve by the routine in Numerical Recipes *NR::sor*. With the over-relaxation parameter $\omega = 1$. $\rho_{jac} = \cos\left(\frac{\pi}{32}\right)$. Initially, $u = 0$ everywhere, then at each time step, the interior values of u will be updated. The iteration stops when the following criterion is satisfied:

$$\sum_{j,l} |u_{j+1,l} + u_{j-1,l} + u_{j,l+1} + u_{j,l-1} - 4u_{j,l} - \rho_{j,l}\Delta^2| = \epsilon \sum_{j,l} |\rho_{j,l}\Delta^2|$$

which I set $\epsilon = 10^{-13}$, or the iteration would stop when the number of iterations exceeds 1000. If that is the case, that says the convergence is too slow, and some adjustment of parameters would be required. As a test of the solution to the PDE, the following quantity is computed:

$$F_{j,l} = u_{j+1,l} + u_{j-1,l} + u_{j,l+1} + u_{j,l-1} - 4u_{j,l}$$

If the code works properly, we would expect $F_{j,l} = \rho_{j,l}\Delta^2$. So, at the center grid point, the value takes $2\Delta^2 \simeq 0.001953125$, and zero everywhere. See Tables 1.1 and 1.2 at the back for values of $u_{j,l}$ and $F_{j,l}$ on the grids. (With spacing 4Δ shown for brevity). On the upper left, $j = 0 = l$. $j(x)$ increases to the right, while $l(y)$ increases downwards.

2 Non-linear Elliptic PDE

Solve

$$\frac{\partial^2 u}{\partial x^2} + \frac{\partial^2 u}{\partial y^2} + u^2 = \rho$$

with the same boundary conditions and $\rho(x, y)$ as before. The method to be used to solve this problem is very similar to the previous method, except that, to deal with the non-linear term u^2, it has to be linearized.

$$u_{j,l}^{n+1} \simeq \left(u_{j,l}^n\right)^2 + 2u_{j,l}^n \left(u_{j,l}^{n+1} - u_{j,l}^n\right)$$

Thus, the coefficients of the FD equation would be in general dependent on $u_{j,l}^n$ from the previous time step. After some algebratic manipulation, the finite difference equation is:

$$u_{j,l}^{n+1} = u_{j,l}^n + \left(\frac{-\left[u_{j+1,l}^n + u_{j-1,l}^n + u_{j,l+1}^n + u_{j,l-1}^n - 4u_{j,l}^n\right] \frac{1}{\Delta^2} - \left(u_{j,l}^n\right)^2 + \rho_{j,l}^n}{-\frac{4}{\Delta^2} + 2u_{j,l}^n} \right)$$

The numerical solution of this problem is very similar to Q.1., for the values of u's are of the order of 10^{-3}, so the effect of adding a source term of u^2 is fairly negligible.

Again, $F_{j,l}$ is checked to confirm if the solution indeed satisfies the PDE. We expect this quantity to be equal to $\rho_{j,l}\Delta^2$, by finite differencing the non-linear PDE.

$$F_{j,l} = u_{j+1,l} + u_{j-1,l} + u_{j,l+1} + u_{j,l-1} - 4u_{j,l} + \Delta^2 (u_{j,l}^{n+1})^2$$

Looking at table 2.1, it shows the distribution of $u_{j,l}$ of the non-linear PDE. It is almost identical to table 1.1. To show they are different, tables 2.2 and 2.3 are showing the distribution of $F_{j,l}$ of the non-linear PDE in Q.2., using the modified SOR code (attached), and the distribution of $F_{j,l}$ of the same equation, but using the standard SOR code. Again, spacing of 4Δ is used.

One can see table 2.2 demonstrates a higher accuracy of the numerical solution, showing that different codes were run.

3 Linear Elliptic PDE solved by full multigrid method

The same equation in Q.1. is solved by the full multigrid method instead. The Numerical Recipes routine *NR::mglin* is used. The same checks for the solution are performed and are shown in Table 3.1 ($u_{j,l}$) and 3.2 ($u_{j,l}$). I am showing $F_{j,l}/\Delta^2$ instead. Again, spacing of 4Δ is shown.

For the same grid resolution, the full multigrid method runs much faster than the SOR code. For instance, for 32×32 square lattice, the multigrid method takes 0.0053 s to run, yet the SOR code takes 0.0273 s to run.

4 Fast Fourier Transform

4.1 FFT

The Gaussian function $h(t) = \exp(-t^2)$ is sampled at N discrete points. To see how different sampling rates affect the accuracy of the numerical solution, I tried $N = 32$, 128 and 512 respectively. N has to be some integers of power of 2, for the FFT code in Numerical Recipes to work.

$$t_i = -10 + 20\left(\frac{i}{N}\right) \qquad (-10 \le t < 10)$$
$$h_i = \exp\left(-t_i^2\right)$$

Looking at the exponential function, $|t| \approx 10$ is essentially effective to ∞.

To solve this problem, the routine *NR::four1* is used to perform the FFT. The FFT spectrum is defined in the frequency space from $f = 0$ to $f = n/N$ (in the unit of $1/\Delta$, where $\Delta = 20/N$, $n = 0, \ldots, N$. For the range of $N/2 < f \le N$, they correspond to the negative frequency spectrum, which I have flipped to negative frequencies as shown in Figs. 1, 2 and 3).

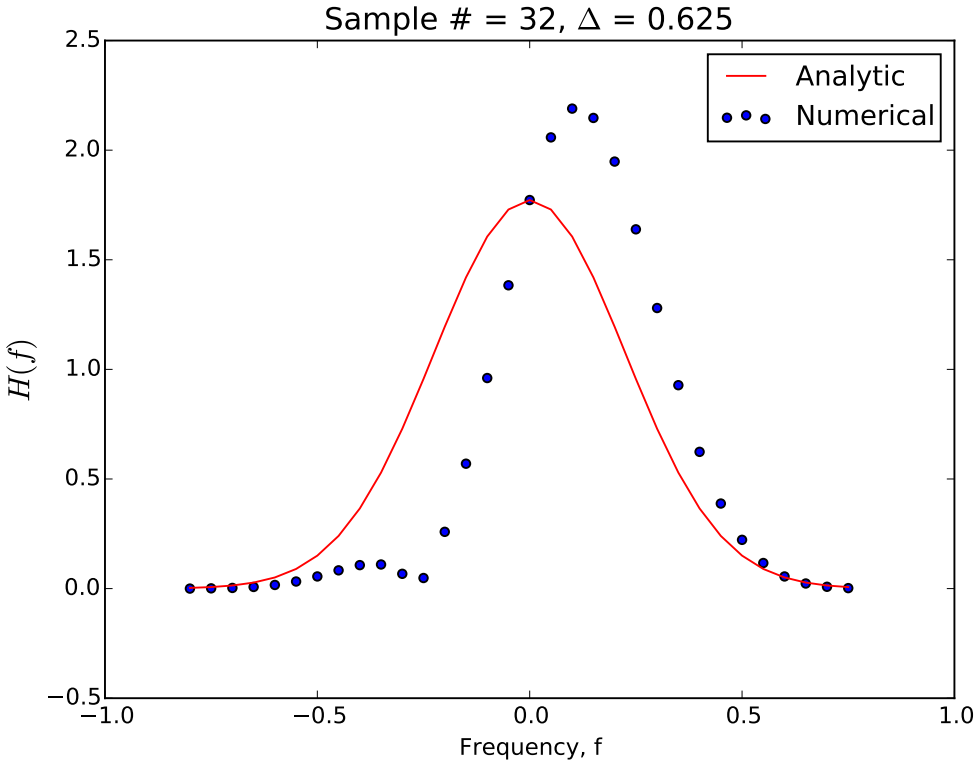

Figure 1: Fourier transform of $h(t) = \exp(-t^2)$, with $N = 32$, $\Delta = 0.625$.

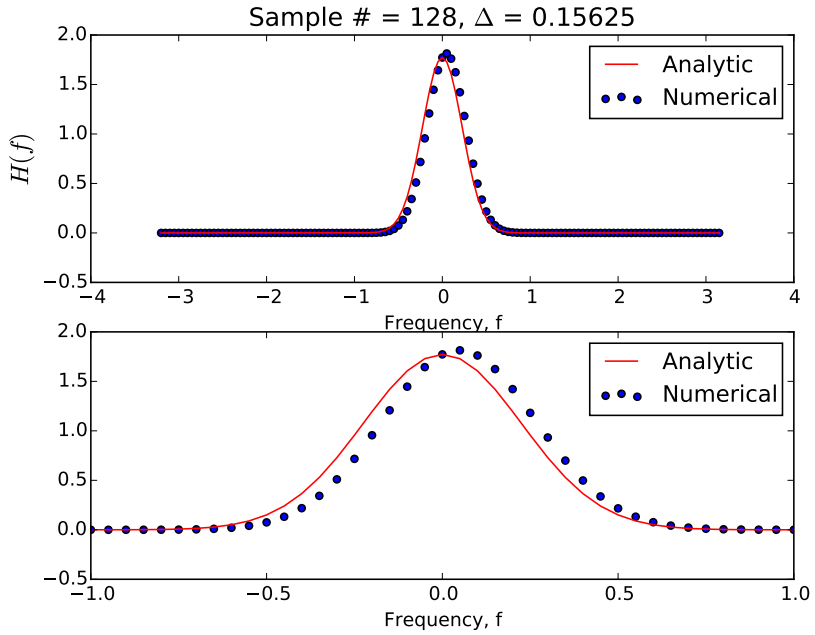

Figure 2: Fourier transform of $h(t) = \exp(-t^2)$, with $N = 128$, $\Delta = 0.15625$. Top: Whole spectra. Bottom: $-1 \leq f \leq 1$.

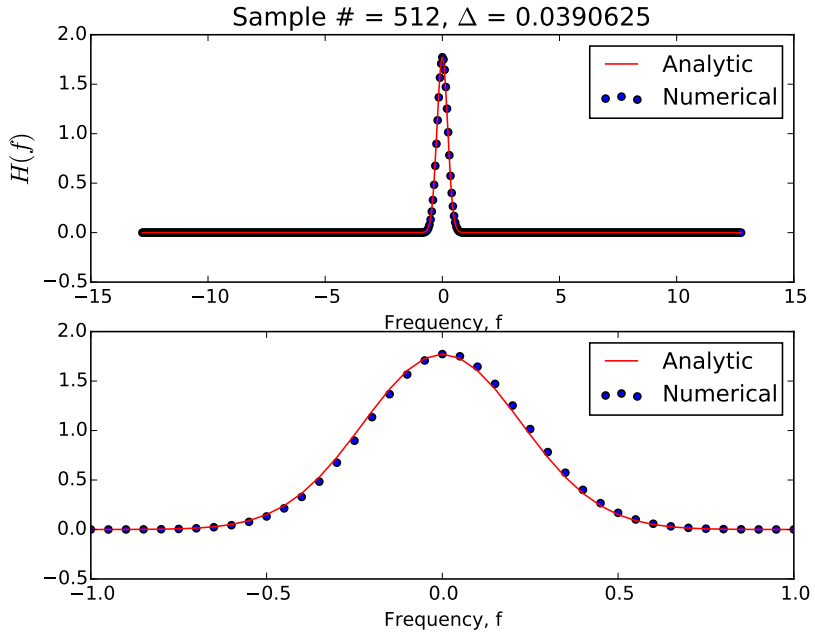

Figure 3: Fourier transform of $h(t) = \exp(-t^2)$, with $N = 512$, $\Delta = 0.0390625$. Top: Whole spectra. Bottom: $-1 \leq f \leq 1$.

As seen in Figs 1, 2 and 3, the higher the sampling rate (The higher N), the better the fit is. In Fig. 1 ($N = 32$), the FFT could roughly fit the shape of the analytical solution $H(f) = \pi^{1/2} \exp(-\pi^2 f^2)$, yet there is still some deviation from the analytical solution.

As the sampling rate gets higher (Figs. 2 ($N = 128$), 3 ($N = 512$)), the fit of the numerical solution is better. The top panels of the figures show the fit of the numerical solution to the analytic form. The bottom panels are the zoomed-in figures. As expected, ($N = 512$) gets an even better fit than ($N = 128$).

The characteristic frequency of the spectrum is $f_0 = 1/\pi \simeq 0.32$. So for $N = 32$, $f_c = 1/2\Delta = 0.8$, which is about the same order of the characteristic frequency. The effect of aliasing might deteriorate the numerical fit to the analytical solution. For higher N's, the sampling frequencies are much higher than the Nyquist frequency, so the fit would be much better.

4.2 Inverse FFT

The inverse Fourier Transform of $H(f)$ is taken in discrete Fourier transform, and is compared with the original discrete sample. Again, the higher the N's are, the more accurate the inverse transform is. But for the three frequencies, all information is preserved (The shapes preserve).

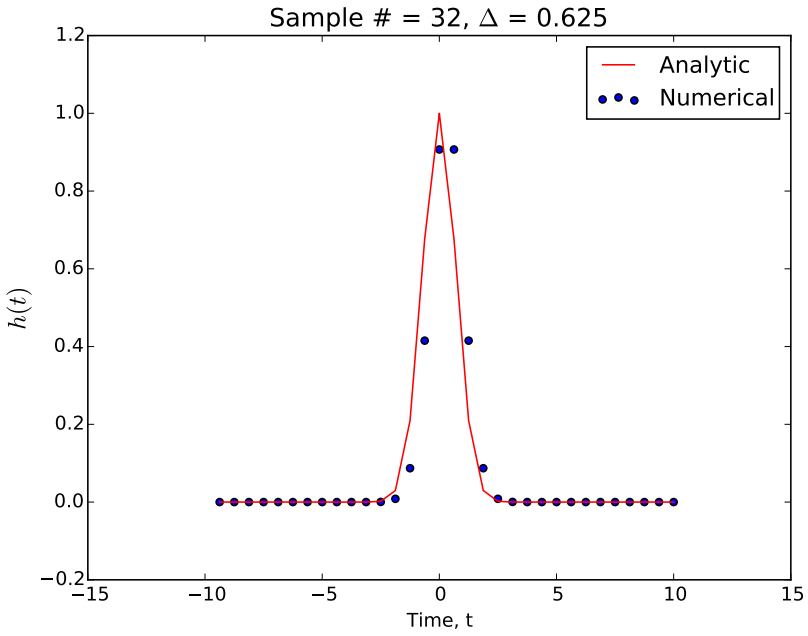

Figure 4: Inverse Fourier transform of $H(f) = \pi^{1/2} \exp(-\pi^2 f^2)$, with $N = 32$, $\Delta = 0.625$.

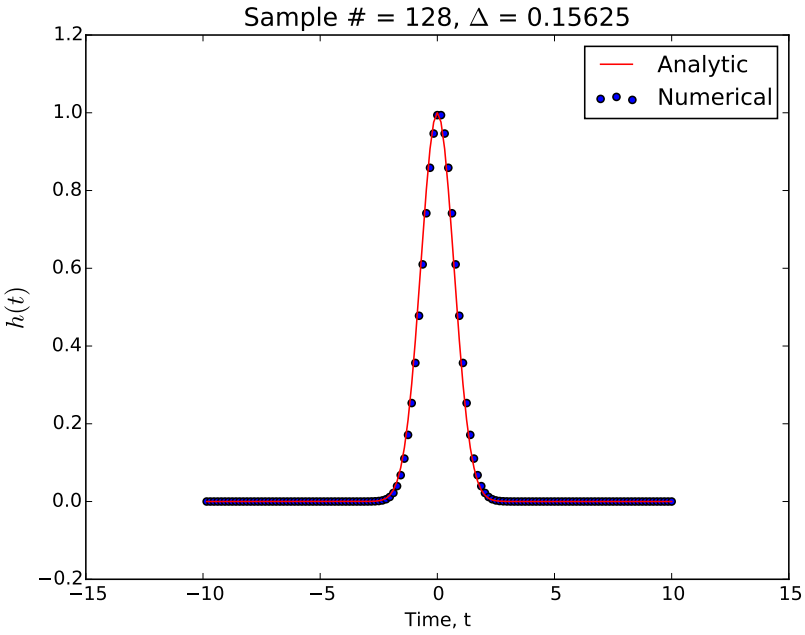

Figure 5: Inverse Fourier transform of $H(f) = \pi^{1/2} \exp(-\pi^2 f^2)$, with $N = 128$, $\Delta = 0.15625$.

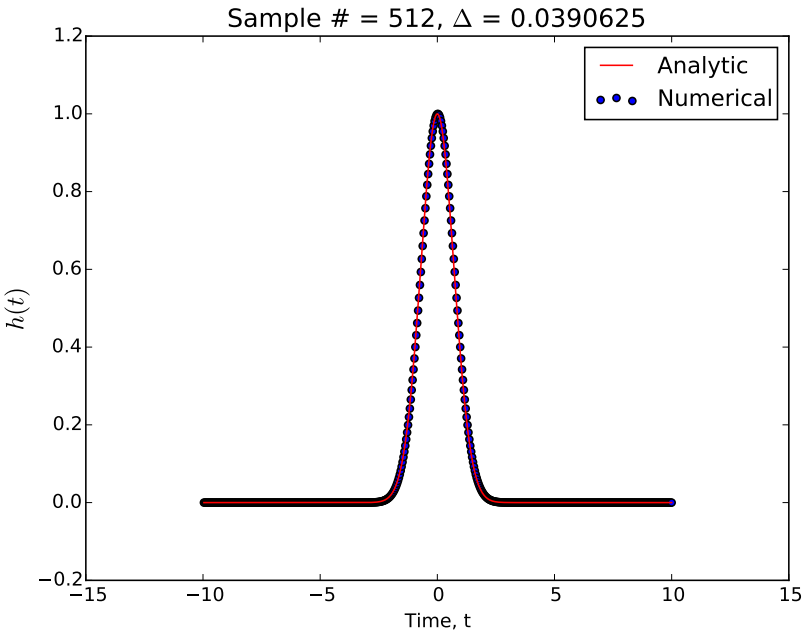

Figure 6: Inverse Fourier transform of $H(f) = \pi^{1/2} \exp(-\pi^2 f^2)$, with $N = 512$, $\Delta = 0.0390625$.

5 Did not do

6 Pendulum Analysis

Perform an FFT on the data in problem set 6, for two sets of parameters, (i). $(q, b, \omega_0) = (0.5, 0.9, 2/3)$ and (ii). $(q, b, \omega_0) = (0.5, 1.15, 2/3)$. The one-sided power spectrum are constructed by computing $P(\omega) = 2|H(\omega)|^2$, where $\omega = 2\pi f$ and $H(\omega)$ are the Fourier transforms. I performed the fourier transforms on the data with respect to $\theta(t)$ and $d\theta/dt(t)$ respectively, the two power spectrum agree with each other which shows the code does indeed work. In both cases, $\omega_0 = 2/3$.

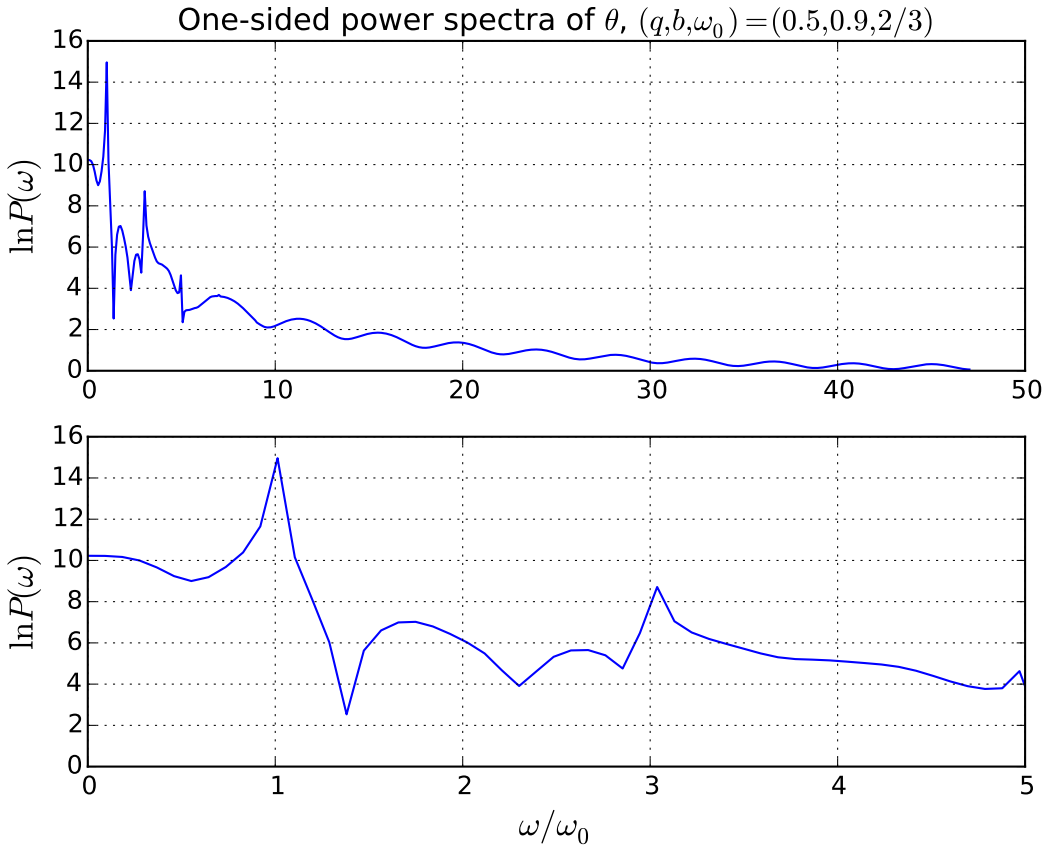

Figure 7: The one-sided power spectrum of $\theta(t)$ for the parameters $(q, b, \omega_0) = (0.5, 0.9, 2/3)$. Top: Whole power spectrum. Bottom: Zoomed-in power spectrum for $0 \leq \omega/\omega_0 \leq 5$. The power spectrum peaks at $\omega/\omega_0 \approx 1$, showing the motion is dominated by this frequency.

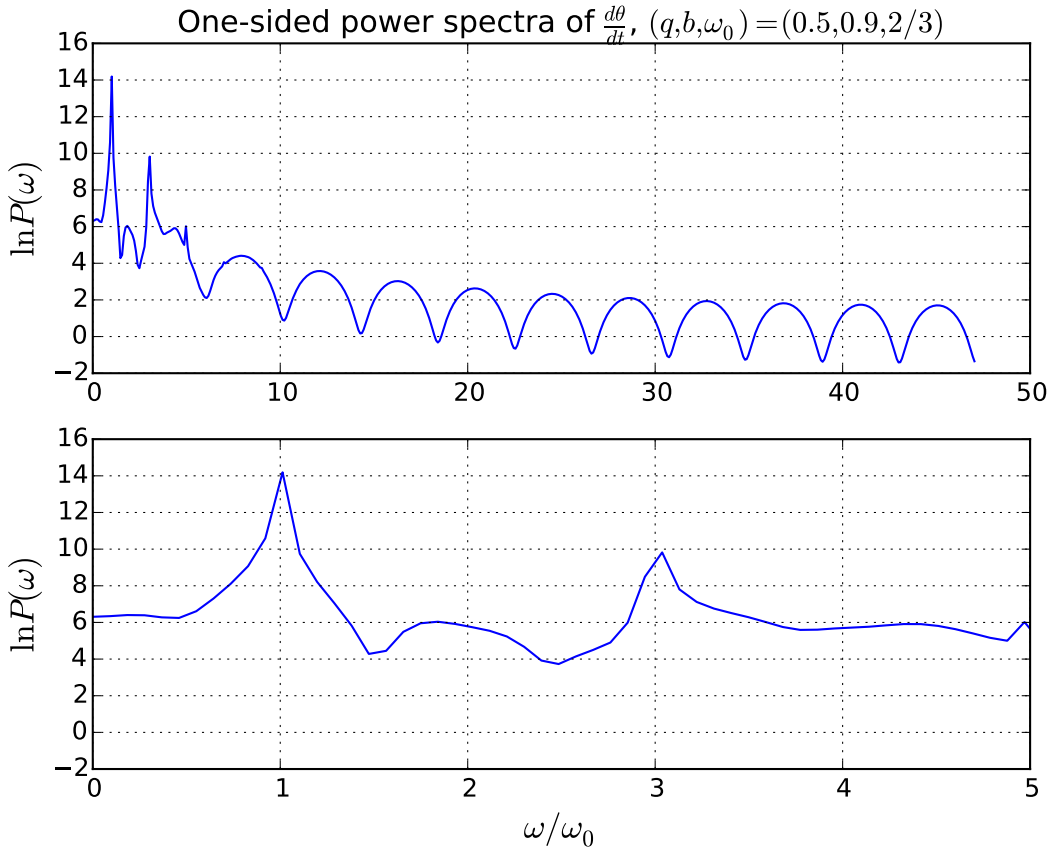

Figure 8: The one-sided power spectrum of $d\theta(t)/dt$ for the parameters $(q, b, \omega_0) = (0.5, 0.9, 2/3)$. Top: Whole power spectrum. Bottom: Zoomed-in power spectrum for $0 \leq \omega/\omega_0 \leq 5$. This plot agrees with Fig. 7, showing the peak frequency is at $\omega/\omega_0 \approx 1$.

Figs. 7 and 8 show that the power spectrum peak at $\omega/\omega_0 \approx 1$. The two plots agree with each other on locating the peak frequency (dominant frequency of oscillation). This is further confirmed by Fig. 9, which the period of the motion is about 10s. It corresponds to the frequency of $\omega = 0.2\pi = 0.63 \approx 2/3$, which agrees that the dominant frequency is indeed $\omega/\omega_0 \approx 1$.

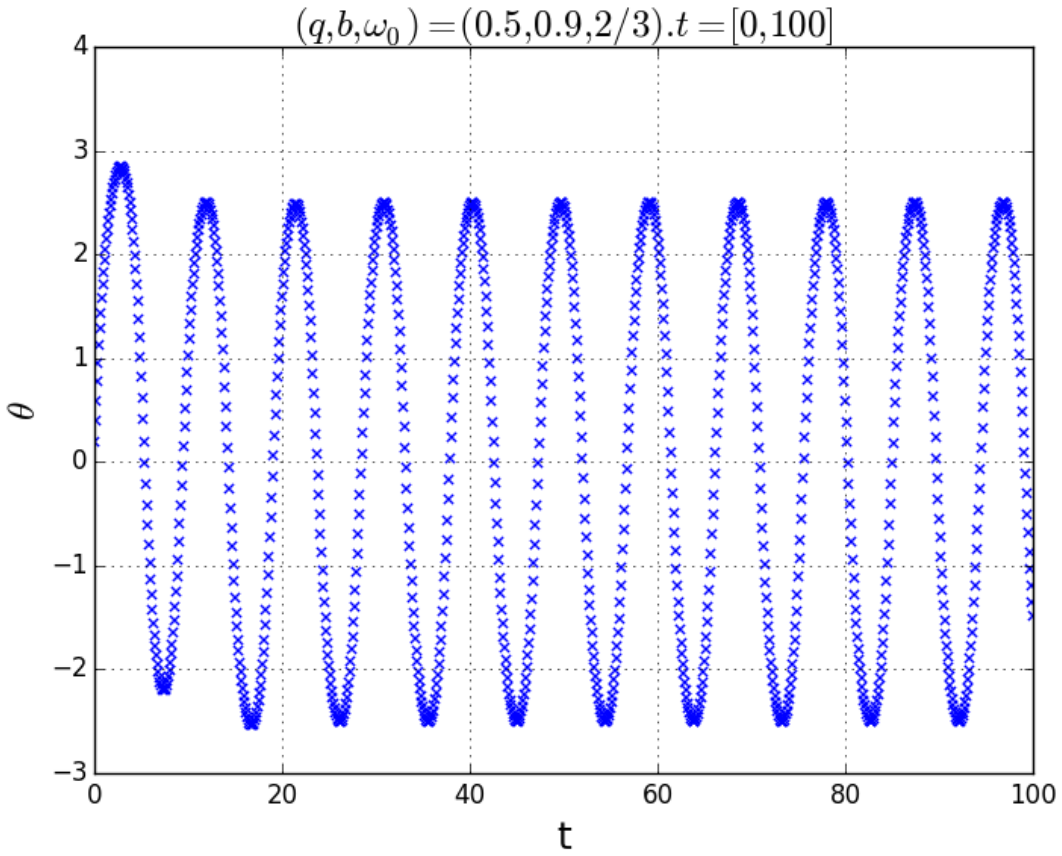

Figure 9: $\theta(t)$ v.s. t for the parameters $(q, b, \omega_0) = (0.5, 0.9, 2/3)$. This plot shows the period of the oscillation is about $t = 10s$, which corresponds to $\omega = 0.2\pi = 0.63 \approx 2/3$, so the oscillation is indeed dominated by $\omega/\omega_0 \approx 1$, confirming Figs. 7 and 8.

For the parameter set of $(q, b, \omega_0) = (0.5, 1.15, 2/3)$, the motion is chaotic (from problem 6, Figs. 12 and 13 are shown for reference.) The one-sided power spectrum (Figs. 10 and 11) show that there is not a dominant frequency (or the spectrum peak at $\omega/\omega_0 = 0$).

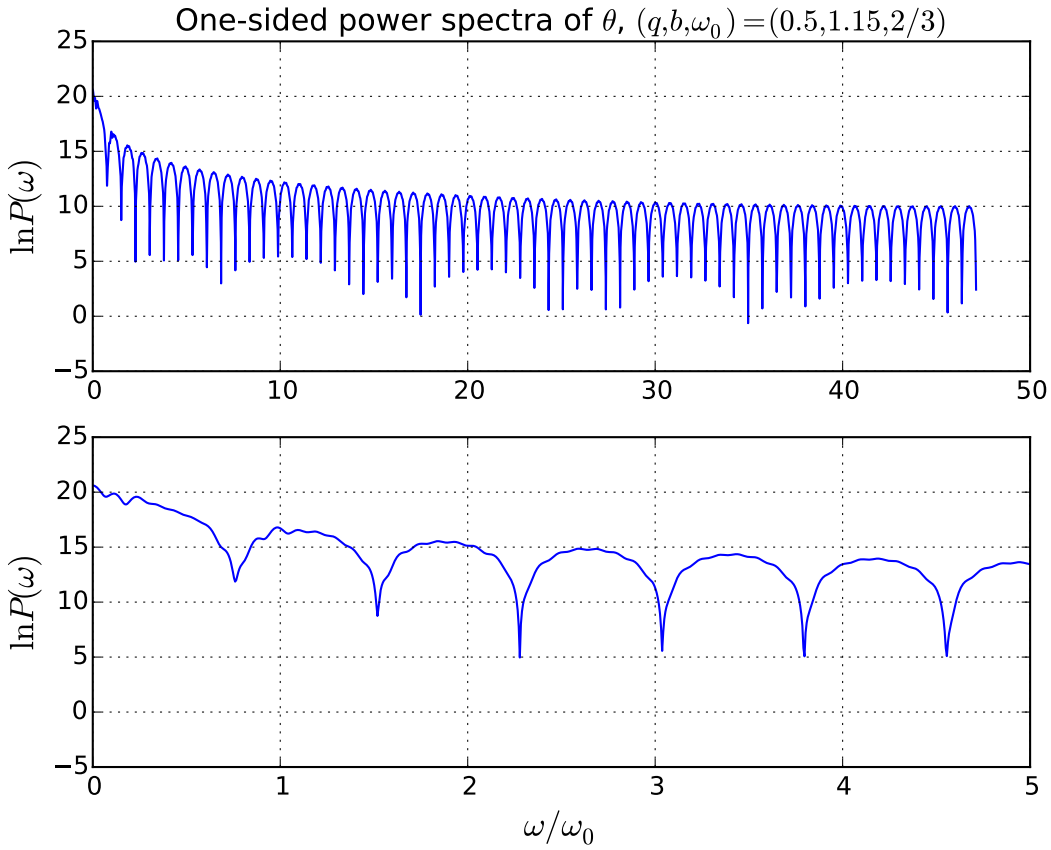

Figure 10: The one-sided power spectrum of $\theta(t)$ for the parameters $(q, b, \omega_0) = (0.5, 0.9, 2/3)$. Top: Whole power spectrum. Bottom: Zoomed-in power spectrum for $0 \leq \omega/\omega_0 \leq 5$. The peak frequency is at $\omega/\omega_0 \approx 0$, as the motion is chaotic, no periodicity can be well-defined.

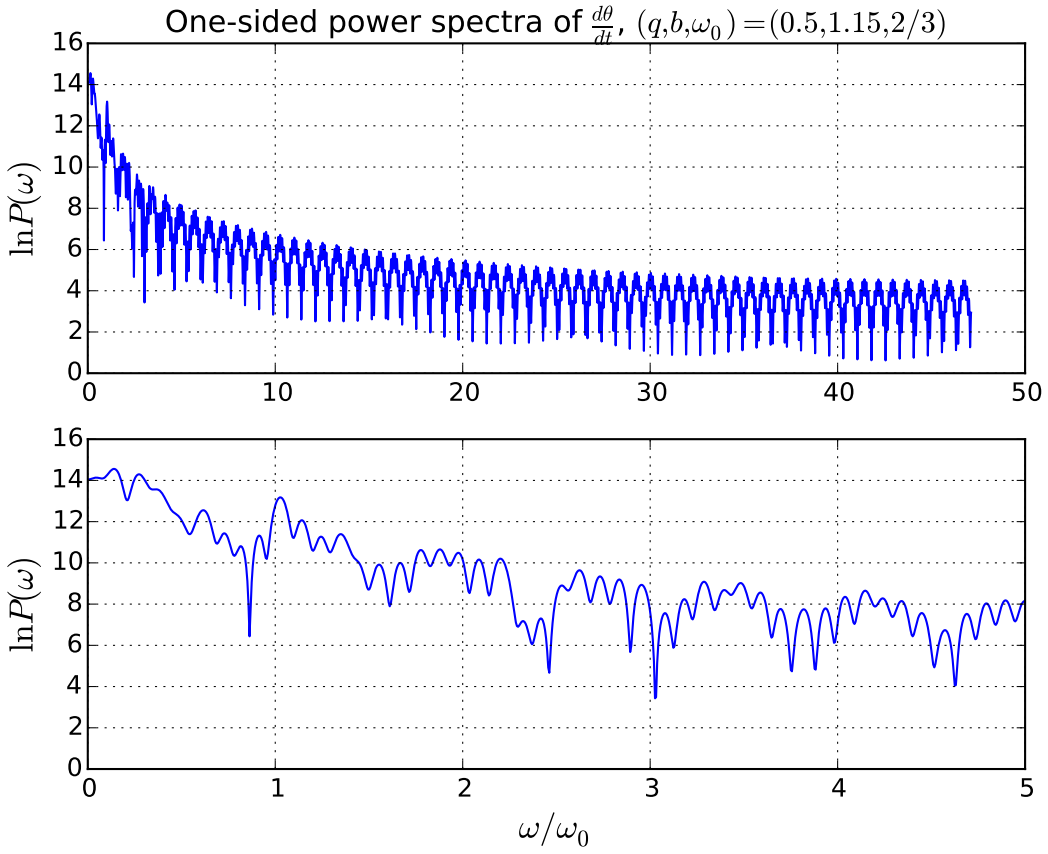

Figure 11: The one-sided power spectrum of $d\theta(t)/dt$ for the parameters $(q, b, \omega_0) = (0.5, 0.9, 2/3)$. Top: Whole power spectrum. Bottom: Zoomed-in power spectrum for $0 \leq \omega/\omega_0 \leq 5$. This plot agrees with Fig. 10, showing the motion is chaotic.

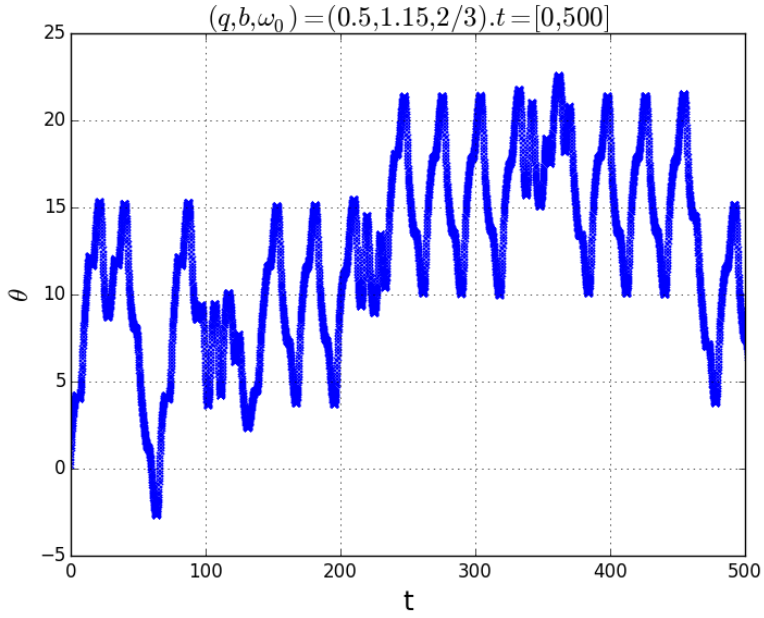

Figure 12: $\theta(t)$ v.s. t for the parameters $(q, b, \omega_0) = (0.5, 1.15, 2/3)$. This plot shows the oscillation is chaotic, no periodicity can be defined. Thus confirming the finding of Figs. 10 and 11.

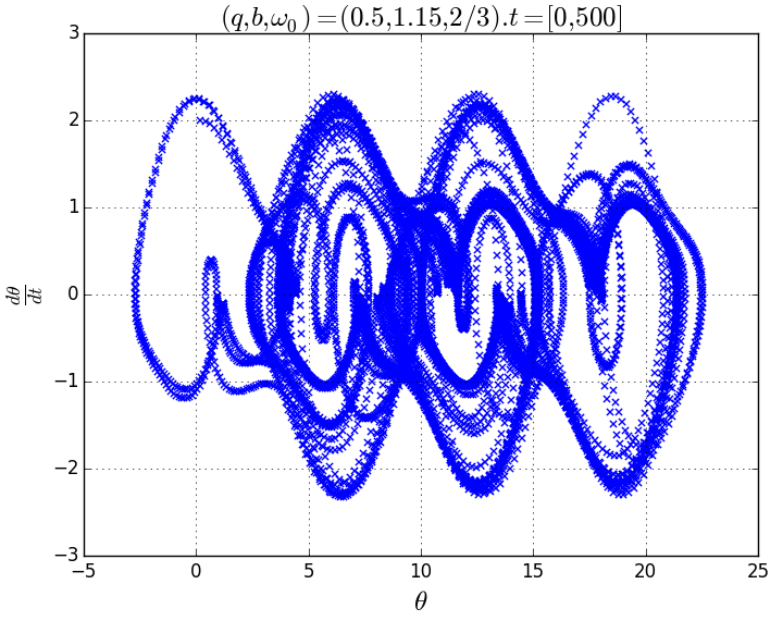

Figure 13: Phase diagram of the motion for the parameters $(q, b, \omega_0) = (0.5, 1.15, 2/3)$. This confirms with Figs. 10, 11 and 12.